Biosensors and Bioelectronics 70 (2015) 351–357

Contents lists available at ScienceDirect

Biosensors and Bioelectronics

journal homepage: www.elsevier.com/locate/bios

Ultrasensitive electrochemical detection of microRNA-21 combining layered nanostructure of oxidized single-walled carbon nanotubes and nanodiamonds by hybridization chain reaction

Lingzhi Liu [1], Chao Song [1], Zhang Zhang, Juan Yang, Lili Zhou, Xing Zhang, Guoming Xie *

Key Laboratory of Laboratory Medical Diagnostics of Ministry of Education, Department of Laboratory Medicine, Chongqing Medical University, Chongqing 400016, PR China

ARTICLE INFO

Article history:
Received 18 December 2014
Received in revised form
7 March 2015
Accepted 21 March 2015
Available online 28 March 2015

Keywords:
MicroRNA-21
Oxidized single-walled carbon nanotubes
Nanodiamonds
Tetrahedron-structured probes
Hybridization chain reaction

ABSTRACT

Measurement of microRNA (miRNA) levels in body fluids is a crucial tool for the early diagnosis and prognosis of cancers. In this study, we developed an electrochemical assay to detect miRNA-21 by fabricating the electrode with layer-by-layer assembly of oxidized single-walled carbon nanotubes and nanodiamonds. Tetrahedron-structured probes with free-standing probe on the top served as receptors to hybridize with target miRNA directly. The probes were immobilized on the deposited gold nanoparticles through a well-established strong Au–S bond. The electrochemical signal was mainly derived from an ultrasensitive pattern by combining hybridization chain reaction with DNA-functionalized AuNPs, which provided DNAzyme to catalyze H_2O_2 reduction. Differential pulse voltammetry was applied to record the electrochemical signals, which was increased linearly with the target miRNA-21, and the linear detection range was 10 fM to 1.0 nM. The limit of detection reached 1.95 fM (S/N=3), and the proposed biosensor exhibited good reproducibility and stability, as well as high sensitivity. Hence, this biosensor has a promising potential in clinical application.

1. Introduction

MicroRNAs (miRNAs) have emerged as new biomarkers in cancer diagnostics and prognostics, which play a considerable role in regulating the expression of target genes as proto-oncogene or tumor-suppressor in humans (Zhang et al., 2014). Moreover, deregulations of miRNAs are associated with various human cancers, such as lung, brain, colon, breast cancer, and leukemia (Yin et al., 2013). Accordingly, finding an appropriate method to detect miRNAs in body fluids has attracted much attention worldwide. Structurally, miRNAs are a class of highly conserved non-coding RNA molecules and consist of 19 to 24 nucleotides (Shi et al., 2014, Ryoo et al., 2013). Owing to the extremely similar sequences and low expression, establishing a method that can identify and quantify miRNAs remains a challenge. More recently, miRNA-21 has been reported to be directly related to the occurrence and development of various cancers; thus, miRNA-21 has been regarded as the excellent biomarker in diagnostic and therapy for cancers (Tian et al., 2013, Ghasemi et al., 2013). Therefore, tremendous progresses have been developed to detect the specific molecule miRNA-21 and realize a stable and sensitive process to make a definite diagnosis in the early stage.

To date, many strategies for detecting miRNAs mainly include Northern blot analysis (Kristina et al. 2013), reverse transcription polymerase chain reaction (Peltier and Latham, 2008), surface plasmon resonance (Zhou et al., 2011), and chemiluminescene (Bi et al., 2011); in particularly, Northern blot analysis is considered the gold standard for identification and quantification. However, these techniques are time consuming, sophisticated, and expensive, then rapidity is needed. Therefore, electrochemical biosensor is elected as the fascinating method due to its simple, rapid, and portable devices for point-of-care tests.

A three-dimensional (3D) layer-by-layer nanostructure, composed of oxidized single-walled carbon nanotubes (SWCNTs-ox) and nanodiamonds (NDs) on the electrodes, expands the surface areas and promotes electron transfer of the biosensor (Singh et al., 2013). SWCNTs-ox with excellent conductivity and special structural feature has attracted extensive attention (Bai et al., 2012). Moreover, NDs not only exhibit the advantages of diamond, but also show superior characteristics of nanomaterials, such as high adsorption capacity and small size (Ermakova et al., 2013), which enlarge the interface areas of SWCNTs-ox layers.

At the same time, we take advantages of tetrahedral DNA

* Corresponding author. Fax: +86 23 68485240.
E-mail address: guomingxie@cqmu.edu.cn (G. Xie).
[1] The authors contributed equally to this work and should be considered as co-first authors.

http://dx.doi.org/10.1016/j.bios.2015.03.051
0956-5663/

nanostructure anchored at the surface of the deposited AuNPs (depAu) as the biosensor platform to meet the requirements of hybridizing more target miRNAs. Tetrahedral DNA architectures have attracted intense interest in this field because of their proven mechanical rigidity and structural stability, as well as the provided effective scaffolds for anchoring of a variety of targets (Pei et al., 2013; Bu et al., 2011). Fan's group has constructed tetrahedron-structured probes (TSPs) successfully, which could be strongly anchored at depAu surfaces through the modified three thiol groups at the vertices, and left a free-standing probe at the top (Pei et al., 2010). TSPs have been proven to be well-ordered and have high distance controllability, by virtue of which the "super-sandwich mode" is created to detect miRNA-21.

The signal units are composed of DNA-functionalized AuNP-based hybridization chain reaction (HCR), which could introduce the superior signal enhancement (Huang et al., 2013). The recently reported hemin-G-quadruplex has become an attractive tool for the amplifying detection of analytes, owing to its significant advantages, such as easy labelling, simple synthesis, and high chemical stability against hydrolysis and heat treatment (Yuan et al., 2013; Zhou et al., 2013). Hemin-G-quadruplex, as a typical DNAzyme, has been shown to exhibit electrocatalytic activity towards H_2O_2-mediated oxidation (Dong et al., 2012). To enhance the immobilization amount of hemin-G-quadruplex, HCR, an isothermal amplification technique that depends on the autonomous self-assembly of short DNA fragments through specific interactions, was used to fabricate long hemin-G-quadruplex DNAzyme nanowires. Moreover, HCR is an enzyme-free process; the initiator strand (helpter) propagated a cascade of hybridization events between alternating auxiliary probe 1 (AP1), auxiliary probe 2 (AP2), and auxiliary probe 3 (AP3) to yield a 3 D DNA concatemers. Their branched 2D or 3D analogues-DNA dendrimers have been employed to amplify the signal and improve the trapping of query nucleic acids in the hybridization analysis (Liu et al., 2014; Huang et al., 2013). DNA-functionalized AuNPs are modified with the long hemin-G-quadruplex DNAzyme nanowires, resulting in

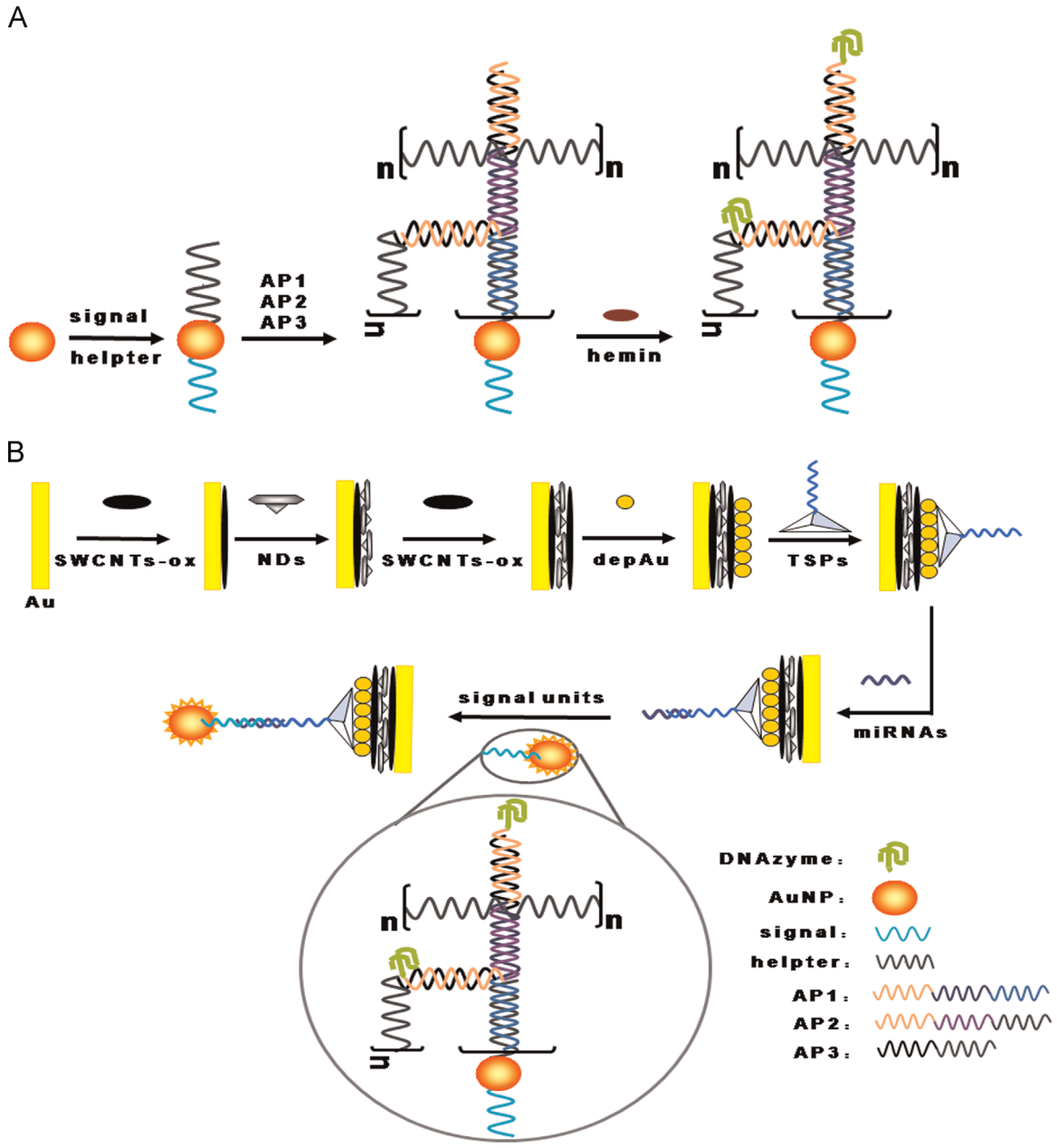

Scheme 1. Schematic illustrations of the electrochemical biosensor. Note: n represents the number of cycles.

remarkably amplified final electrochemical signal (Zhang et al., 2012).

In the present study, we created a novel electrochemical biosensor to detect miRNA-21 via a highly stable and ultrasensitive method (Scheme 1).

2. Experimental

2.1. Reagents

All oligonucleotides, 1 × TE, and sodium dodecyl sulfate (SDS) were obtained from Shanghai Sangon Biological Engineering Technology and Services Co. (Shanghai, China), and all oligonucleotides are illustrated in Table S1. Hemin, chloroauric acid ($HAuCl_4$), and tri(2-carboxyethyl) phosphine hydrochloride (TCEP) were purchased from Sigma-Aldrich Trading Co. (MO, USA). SWCNTs-ox and NDs were purchased from the Pioneer Nanotechnology Co. (Nanjing, China). 20 bp DNA Ladder Marker and agarose were purchased from TaKaRa Biotechnology Co. (Dalian, China). Tris–HCl solution (pH 7.4), containing 300 mM NaCl and 1 mM $MgCl_2$, and phosphate buffer solution (PBS) containing 0.5 M NaCl were used in the experiment. Saline sodium citrate (2 × SSC) buffer (pH 7.5), containing 30 mM sodium citrate and 300 mM NaCl, was used as hybridization solution. Ultrapure water (Milli-Q 18.2 MΩ) and double distilled water were used in the experiments.

2.2. Apparatus

All electrochemical experiments were performed in a CHI 660D electrochemistry working station (Shanghai Chenhua Instrument, China). A conventional three-compartment electrochemical cell was employed in all electrochemical measurements, which composed of a modified gold electrode (3 mm) as working electrode, a KCl-saturated Ag/AgCl electrode as reference electrode, and a platinum wire as auxiliary electrode. Scanning electron microscopy (SEM, FEI Nova-400, USA) and transmission electron microscopy (TEM, Hitachi-7500, Japan) were employed for morphological analysis. Atomic force microscopy (AFM, Nano Wizard II, Germany) was used to observe the images of the DNA-functionalized AuNPs. A 1000-series thermal cycling platform (CA, USA) was used to assemble the tetrahedron-structured probes.

2.3. Design principle of DNA-functionalized AuNP-based HCR

Scheme 1a shows the scheme of DNA-functionalized AuNP-based HCR. First, the signal probe and helpter were bound onto the AuNPs by the sulfydryl at the 5' end. The DNA hybridization chain was then initiated by the helpter, and three auxiliary DNA probes, namely AP1, AP2, and AP3, were hybridized with each right region. In this step, the hemin solution was added into the mixture, and the long hemin-G-quadruplex DNAzyme nanowires were obtained. Finally, the hemin-G-quadruplex DNAzyme exhibited electrocatalytic activity towards H_2O_2-mediated oxidation, and the signal units were formed.

2.4. Preparation of gold nanoparticles (AuNPs) and DNA-functionalized AuNPs

Approximately 100 mL of 0.01% (w/v) $HAuCl_4$ was boiled with vigorous stirring. About 2 mL of 1% trisodium citrate was quickly added to the solution. The colloid solution was stirred for another 15 min, and the cooling AuNP solution was stored in a brown flask at 4 °C before use (Mao et al., 2009).

DNA-functionalized AuNPs were prepared according to the previous publication (Xu et al., 2013; Cao et al., 2014) with slight modification. Initially, 0.1 nM signal probe and 0.1 nM helpter were directly dispersed into 500 μL of the above-prepared gold colloids in a 1.5 mL Ep tube (Note: before conjugation, signal probe and helpter should be pretreated by 100-fold excess TCEP at room temperature (RT, 25 °C) for 1 h to split the formed disulfide between the thiolated DNA probes). After gently shaking for 10 min, the mixture was shifted to the refrigerator at 4 °C for further reaction. After incubation, 10 μL of 1% SDS was injected to stabilize the AuNPs, with shaking at RT for 1 h. The resulting solution in 200 μL PBS (0.5 M NaCl, pH 7.4) was aged for 12 h. The solution was then centrifuged at 13,000 rpm for 25 min at 4 °C. The designed as-DNA-AuNPs was washed three times by centrifugation with PBS (0.01 M NaCl, pH 7.4) and then resuspended in 200 μL 2 × SSC hybridization buffer. Afterwards, the solution was incubated into 50 μL of 10 mM Tris–HCl solution, containing 1 μM AP1, 1 μM AP2, and 0.5 μM AP3, for 2 h. The mixture was washed three times by centrifugation with PBS and resuspended in 200 μL 2 × SSC hybridization buffer. About 0.5 mM of hemin solution was then added at RT; the hemin-G-quadruplex DNAzyme was formed after 50 min.

2.5. Self-assembly of DNA tetrahedron-structured probes

Four strands, tetrahedron A, B, C, and D, were dissolved in TE buffer (10 mM Tris, 1 mM EDTA, pH 8.0) up to a final concentration of 50 μM. Approximately 2 μL of each strand was combined with 5 μL of TCEP (30 mM) and 37 μL of TM buffer (20 mM Tris, 50 mM $MgCl_2$, pH 8.0). The mixture was then heated to 95 °C for 5 min, and cooled to 4 °C for over 30 s by using a thermal cycler T-100 (Wen et al., 2011).

2.6. Fabrication of the biosensor

For the layer-by-layer preparation of SWCNTs-ox and ND nanostructure approaches, the pretreated electrode was modified with 10 μL of SWCNTs-ox (0.1 mg mL^{-1}) dispersed in ultrapure water by classical casting methods. About 5 μL of ND solution (0.5%) dispersed in H_2O_2: ethanol (1:1) solvent was then deposited on the SWCNTs-ox layer. Furthermore, another SWCNTs-ox layer was deposited as described previously. The modified electrode was dried and immersed in $HAuCl_4$ solution for electrochemical deposition of AuNPs. Subsequently, 5 μL of TSPs was dropped on the formed electrode at RT overnight. After each step, the modified electrode was swilled thoroughly with double distilled water to prevent the non-chemisorption. The finished biosensor was stored at 4 °C before use.

2.7. Electrochemical measurements

In this work, the resulting biosensors were incubated with different concentrations of miRNA-21 for 1 h at 37 °C, respectively. The signal probe on the DNA-functionalized AuNPs was transduced to "surpersandwich mode" and final DNAzyme turnover-based signal transduction. The electrochemical measurement with differential pulse voltammetry (DPV) was performed in 0.1 M PBS (pH 7.0) containing 20 mM H_2O_2. All measurements were conducted at RT.

The standards were prepared with different concentrations of miRNA-21. Blood specimens were gifted by the First People's Hospital, Jiulongpo District of Chongqing.

3. Results and discussion

3.1. Characteristics of the different nanomaterials

The TEM images in Fig. 1A provide the size and morphology of the citrate-reduced AuNPs. The well-dispersed particles with a diameter of ~16 nm were suitable for nucleic acid labeling. The conjugation of the signal probe and initiator strand helpter on the AuNPs led to a large particles diameter and blunt images (Fig. 1B) (Zhou et al., 2013). In particularly, the particles remained separated with each other without any aggregation, thus implying good dispersion.

When 1 μM AP1, 1 μM AP2, and 0.5 μM AP3 were incubated for 2 h to generate the HCR, the result was verified with gel electrophoresis experiment (Ge et al., 2014) (Fig. 1C). Without DNA-AuNP, the reaction pool of AP1, AP2 and AP3 could produce three kinds of concatamers (lane 5). The mixtures of 1 μM AP2 and 1 μM AP3, 1 μM AP1 and 1 μM AP2, 1 μM AP1 and 1 μM AP3 could also cause hybridization, respectively. The comparative results were shown in the lanes 6, 7 and 8, and the interference shown at lane 5 might be that there were no helpter-AuNPs and steps of washing by centrifugation when the HCR was acted in the gel electrophoresis experiment. Therefore, the HCR product showed the light brands at about 80 bp and the reaction conditions (reaction time, temperature) had also been adjusted to the optimal state.

To confirm the conjugation of DNA on the AuNPs, the DNA-functionalized AuNPs were monitored by AFM (Ma et al., 2013; Song et al., 2014). Three 3D height maps display AFM images of AuNPs and signal-AuNPs-helpter (Fig. 1). As shown in Fig. 1D, a dense and spiky appearance was observed to demonstrate the well-dispersed AuNPs. The AFM images showed a blunt image and the DNA strands were shown as the dotted line in Fig. 1E because of the bioconjugation of signals and helpters, which indicated that oligonucleotides were immobilized onto the surface of AuNPs and that the DNA-AuNPs were formed successfully. When HCR occurred on the base of the DNA-AuNPs, the AFM images become more continuous (Fig. 1F). At the same time, the typical dotted lines on behalf of the nucleic acid chains of HCR were formed crosswise shown by the arrows.

The formed nanostructures were evaluated using SEM for the layer-by-layer deposition of SWCNTs-ox and NDs on the surface of depAu (Singh et al., 2013), where the SWCNTs-ox and the SWCNTs-ox/NDs/SWCNT-ox interfacial layer were exhibited, as shown in Figs. 2A and 2B, respectively. SWCNTs-ox shown in dry state had a highly dense packaging. After ND modification and the second layer of SWCNTs-ox, the highly dense structure was perturbed in the presence of NDs, which appeared in the SEM images as bright spots (Fig. 2B).

3.2. Characteristics of the modified electrodes

The depAu and TSPs modification steps of the proposed biosensor were investigated by SEM observation. After deposition of AuNPs on the layer-by-layer SWCNTs-ox/NDs/SWCNT-ox nanostructures, spherical nanoparticles with an average diameter of 300 nm were coated on the SWCNTs-ox surface, which can increase the immobilization amount of TSPs during the biosensor preparation. The surface of nanostructures becomes much shaping and polygons (Fig. 2C). The adsorbed depAu demonstrated the efficient π-stacking interactions between AuNPs and SWCNTs-ox.

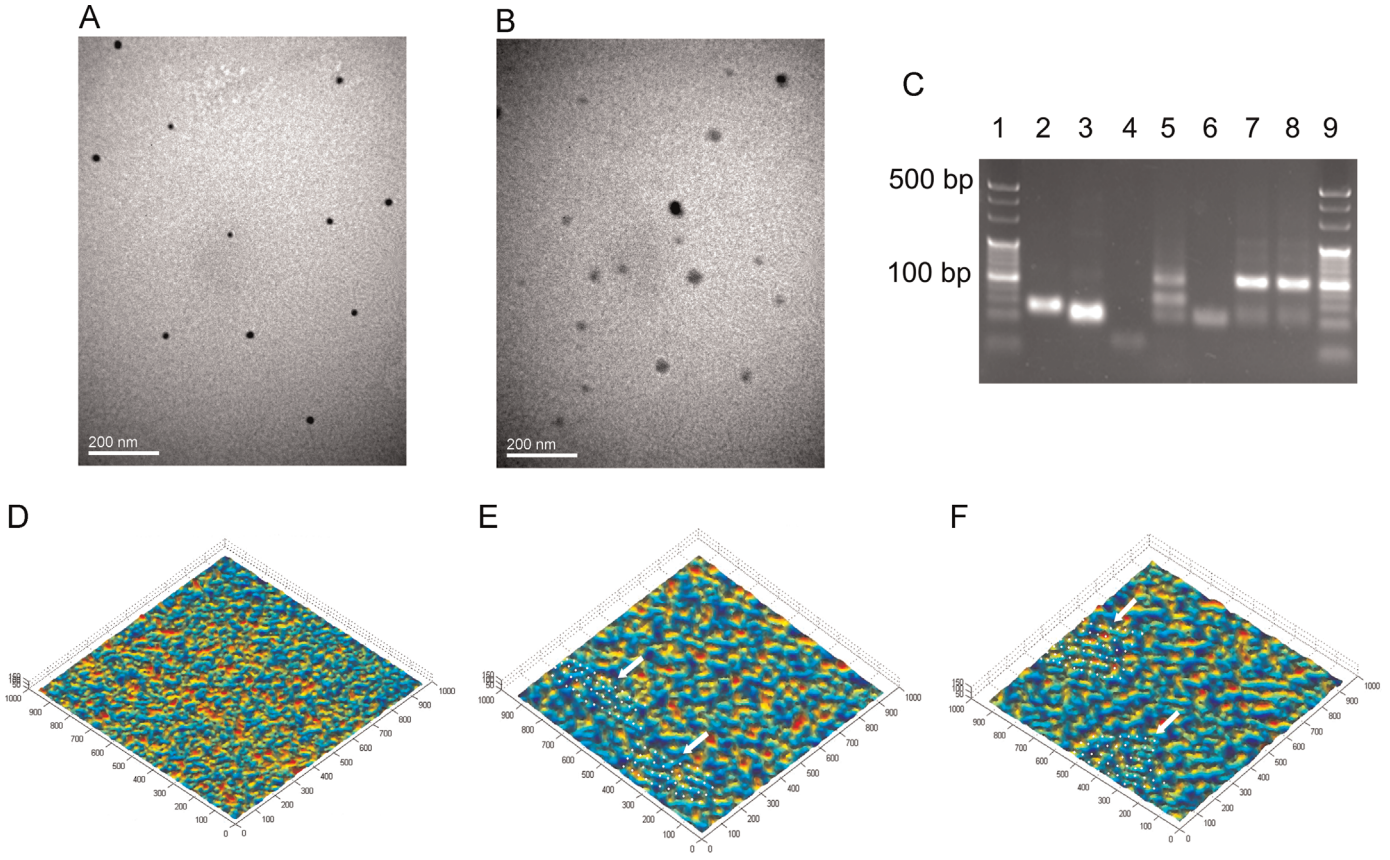

Fig. 1. Transmission electron microscopy (TEM) images of (A) citrate-reduced AuNPs, and (B) conjugation of oligonucleotides and AuNPs. (C) Effect of HCR among auxiliary probe 1 (AP1), auxiliary probe 2 (AP2), and auxiliary probe 3 (AP3). Lanes 1 and 9, 20 bp DNA ladder marker; lane 2, 1 μM AP3; lane 3, 1 μM AP2; lane 4, 1 μM AP1; lane 5, the mixture of 1 μM AP1, 1 μM AP2, and 0.5 μM AP3; lane 6, 1 μM AP2 and 1 μM AP3; lane 7, 1 μM AP1 and 1 μM AP2; lane 8, 1 μM AP1 and 1 μM AP3. Atomic force microscopy (AFM) images of (D) AuNPs, (E) signal-AuNPs-helpter, and (F) HCR at the base of (D).

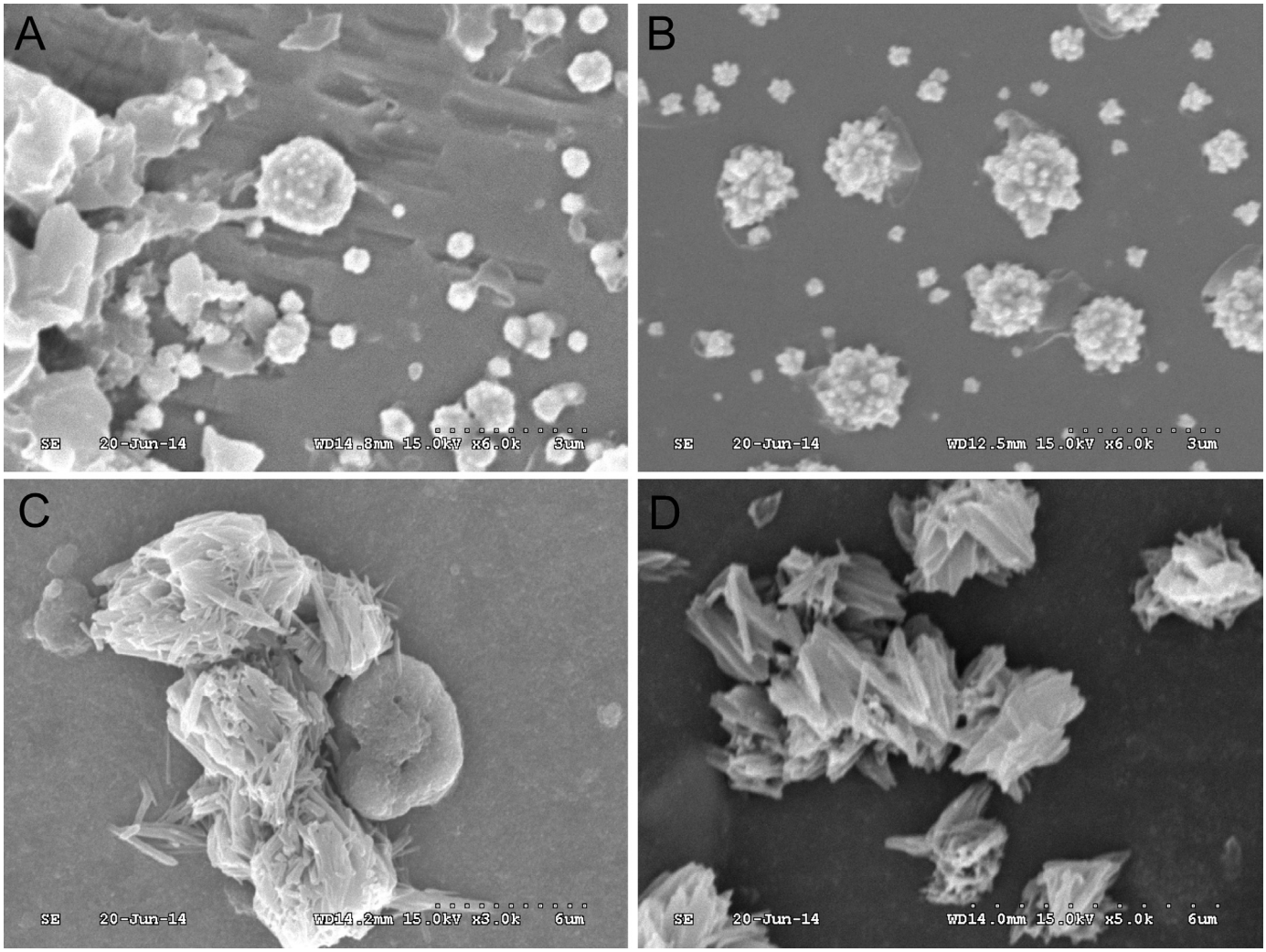

Fig. 2. Scanning electron microscopy (SEM) images of (A) SWCNTs-ox; (B) SWCNTs-ox/NDs/SWCNT-ox; (C) depAu on the SWCNTs-ox/NDs/SWCNT-ox; and (D) TSPs on the surface of depAu/SWCNTs-ox/NDs/SWCNT-ox.

Subsequently, the TSPs were modified after AuNP deposition; evidently, the AuNPs were growing larger, and the surface becomes much rougher. The modified nanostructure exhibits crystal shape (Fig. 2D).

3.3. Electrochemical characterization of the biosensor

The electrode modified with layered nanostructures was monitored by cyclic voltammetry (CV) experiments (Fig. 3A). A pair of well-defined oxidation–reduction peaks was exhibited clearly at the bare Au electrode (curve a). With the addition of SWCNTs-ox, the peak current was increased sharply (curve b), which was attributed to the acceleration of electron transfer. When NDs and the second layer of SWCNTs-ox were deposited on the electrode, the synergistic effect between them facilitated the electron transfer, which demonstrated the assembly of layer-by-layer SWCNTs-ox and that NDs could improve the electrochemical properties remarkably (curves c and d). The peak current increased after AuNP deposition onto the layered nanostructure SWCNTs-ox and NDs, hence suggesting that the conductive depAu could accelerate the electron transfer (curve e).

Thus, the electrochemical characteristics of the biosensor were investigated by EIS measurements shown in Fig. 3B, where the semicircle diameter of EIS is equal to electron transfer resistance (*Ret*). The EIS record of the depAu on the SWCNTs-ox/NDs/SWCNT-ox was curve a. After dropping the TSPs on the modified electrode, *Ret* was enhanced due to the negatively charged phosphate backbone of the tetrahedral DNA nanostructure (curve b). At the same time, the semicircle became small (*Ret* = 1.043 KΩ) compared with the oligonucleotide capture probe modified on the depAu (curve c), thus implying the relatively low resistance of the tetrahedral DNA architectures.

To determine whether the DNA-functionalized AuNP-based HCR reacted through target miRNA-21 to form "supersandwich mode" successfully, the results were monitored by DPV (Fig. 4). Upon the previous steps, miRNA-21 was dropped on the modified electrode, and the current response was recorded as curve a. When signal units with the hemin-G-quadruplex (no H_2O_2) were added, the peak current decreased (curve b). The final catalytic current obtained from the H_2O_2-mediated oxidation reacted with the long hemin-G-quadruplex DNAzyme nanowires (curve c).

3.4. Optimization of experimental conditions

To obtain the perfect performance in the experiment, the optimum conditions of several parameters, such as the concentrations of TSPs, hemin, and H_2O_2, and the HCR reaction time, were optimized by DPV (Fig. S1). These experiments were conducted with the miRNA-21 at 1.0 nM. With increasing TSPs concentrations, the peak current recorded by DPV rose gradually, and

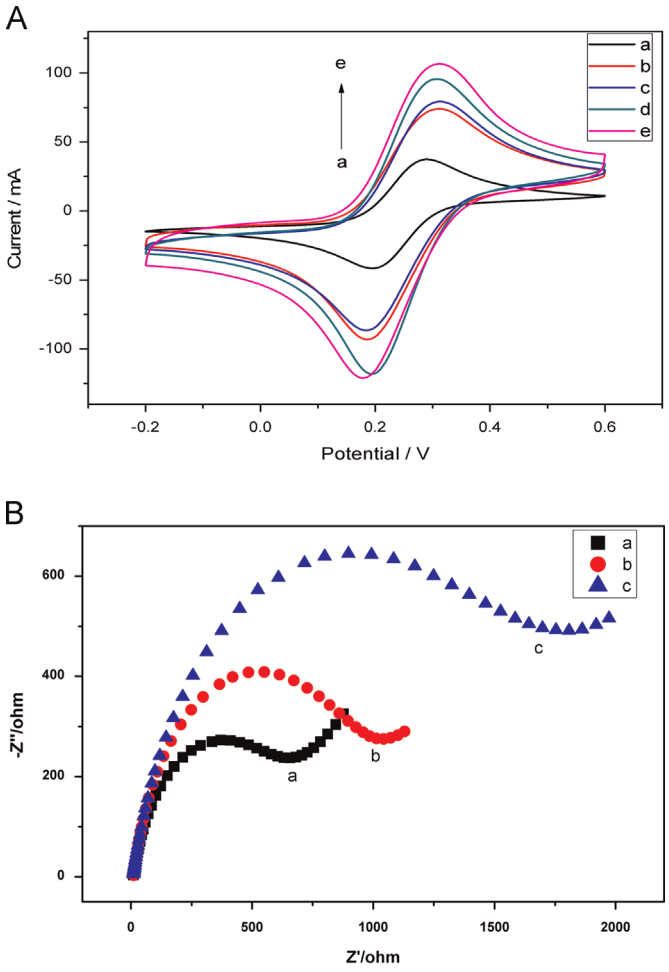

Fig. 3. (A) Cyclic voltammetry (CV) curves of the steps of the fabricated Au electrode: curve a, bare Au electrode; curve b, SWCNTs-ox/Au electrode; curve c, NDs/SWCNT-ox/Au electrode; curve d, SWCNTs-ox/NDs/SWCNT-ox/Au electrode; curve e, depAu/SWCNTs-ox/NDs/SWCNT-ox/Au electrode. (B) The EIS spectra for the modification steps: curve a, depAu/SWCNTs-ox/NDs/SWCNT-ox/Au electrode; curve b, TSPs/depAu/SWCNTs-ox/NDs/SWCNT-ox/Au electrode; curve c, the comparison of oligonucleotide capture probe on the depAu/SWCNTs-ox/NDs/SWCNT-ox/Au electrode. The reaction solution was pH 7.0 phosphate buffer solution containing 5 mM $K_3Fe(CN)_6$ solution containing 0.1 M KCl at a scan rate of 50 mV s^{-1}.

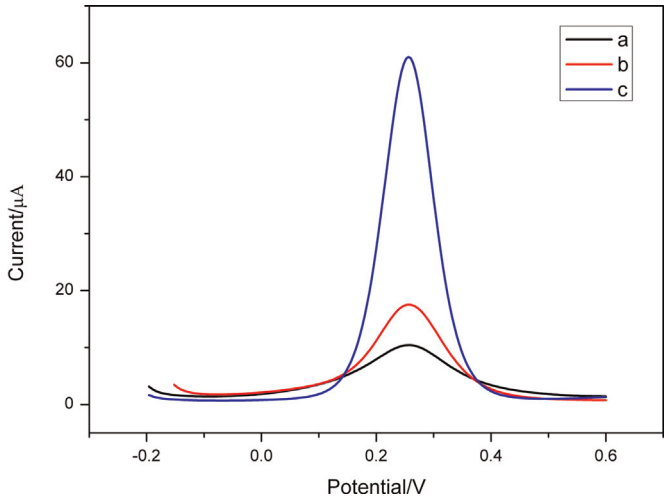

Fig. 4. Differential pulse voltammetry (DPV) response of the biosensor: curve a, after miRNA-21 was hybridized; curve b, signal units with the hemin-G-quadruplex was added; curve c, the H_2O_2-mediated long hemin-G-quadruplex DNAzyme system was added.

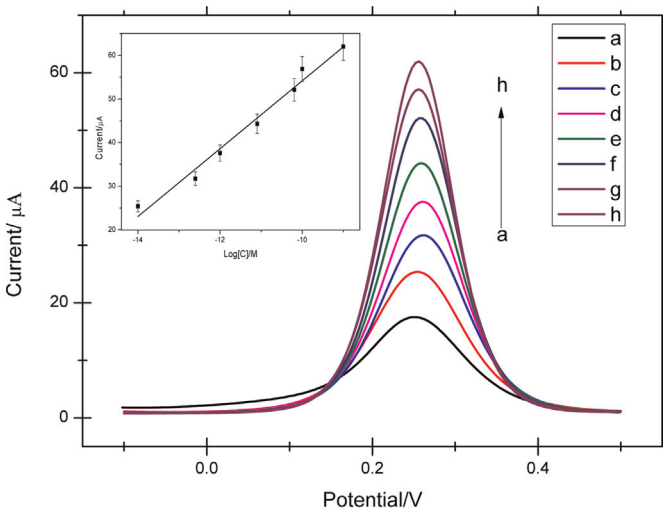

Fig. 5. (A) Calibration curve of the peak current response versus the logarithm of miRNA-21 concentrations by the proposed biosensor. The relative standard deviation (RSD) was 3%. (B) DPV response of the miRNA-21 biosensor with the increasing concentrations of miRNA-21 (from a to h: 0, 1.0×10^{-14}, 2.5×10^{-13}, 1.0×10^{-12}, 8.0×10^{-12}, 6.4×10^{-11}, 1.0×10^{-10}, and 1.0×10^{-9} M).

reached the maximum at 1.0 nM, which was selected as the excellent concentration. The concentration of hemin was modulated from 0.1 mM to 0.6 mM. The current response gradually increased from 0.1 mM to 0.5 mM and reached plateaus at 0.5 mM. The effect of the H_2O_2 concentrations was studied in the range of 10 mM to 30 mM, and the curve reached a plateau after 20 mM. Hence, 20 mM was optimized as the proper H_2O_2 condition during the experiment. The effect of HCR time was also investigated in the range of 30 min to 150 min. The current response increased with HCR time from 30 min to 120 min, and then decreased, and the optimum reaction time was considered 120 min.

3.5. Amperometric response and calibration curve

The signal amplification was confirmed by DPV measurement under optimal conditions. With the concentrations of miRNA-21 decreasing from 1.0 nM to 10 fM (R^2=0.98), the value of peak currents gradually diminished, which generated the calibration curve observed in Fig. 5. Fig. 5 displays a good linear relationship between the logarithm figures of analytes concentration versus the reduction peak currents. The corresponding equation could be expressed as I (μA)=7.7821 log [C/M]+ 131.99, with the low detection limit of 1.95 fM (S/N=3). The peak current values were obtained from the mean value with three independent experiments. These data illustrated that the presence of conductive nanomaterials improved the sensitivity of detecting miRNA-21. The analytical performance of the developed biosensor had been compared with those reported assays in Table S2. The proposed biosensor showed a better performance than others in the analytical range and detection limit.

3.6. Stability, selectivity, and reproducibility

The stability was investigated in this study. When the proposed biosensor was stored in the refrigerator at 4 °C for two weeks, the response remained 91.3%, thus indicating good stability.

Under the optimal conditions, the selectivity of the developed biosensor was checked by detecting single-base mismatch, two-base mismatch, three-base mismatch oligonucleotides, and non-complementary target. The distinguished peak current response of DPV was observed, which is shown in Fig. S2. The results of mismatched sequences were as low as the blank current response.

Equally, the developed biosensor was used in the samples, spiked with other related miRNAs, BSA, and glucose. Nearly negligible current change was observed in the addition of miRNA-126 and miRNA-141 compared with that of the blank. The corresponding DPV response is also shown in Fig. S2. This result reflects that the new biosensor owned high specificity and good selectivity.

To evaluate the reproducibility of the biosensor, five freshly prepared modified electrodes were used to detect the same concentration (1.0 nM) of miRNA-21. All five electrodes exhibited almost similar current response, and the relative standard deviation was 5.1%. The results confirmed the acceptable reproducibility.

3.7. Recovery

Recovery tests were also performed to determine the feasibility of the developed biosensor for clinical applications. Serum samples spiked with miRNA-21 at concentrations of 1.0×10^{-5}, 1.0×10^{-3}, 1.0×10^{-1}, and 1.0 nM were detected using the new biosensor, and the corresponding results are shown in Table S3. The recovery values ranged from 99.3% to 101.6%; thus, the proposed biosensor had potential clinical applicability for the detection of miRNA-21.

4. Conclusion

In summary, our electrochemistry assay provides more specific and sensitive results than other miRNAs detection assays. A new layer-by-layer assembly of SWCNTs-ox and NDs was combined with other nanomaterials to amplify signals. The assembly was applied to modify the electrodes in the rapid and ultrasensitive detection for miRNA-21. Furthermore, TSPs could provide a fine-tuning probe side to hybridize with the miRNAs target. Upon hybridization with DNA-functionalized AuNP-based HCR to construct the “supersandwich mode”, the signal improvement is achieved in the hemin solutions. Finally, the sensitivity of the assay can be recorded by DPV, which is suitable for point-of-care application of miRNAs.

Acknowledgments

This work was financially supported by the Natural Science Research Foundation of China (81171415).

Appendix A. Supplementary material

Supplementary data associated with this article can be found in the online version at http://dx.doi.org/10.1016/j.bios.2015.03.051.

References

Ermakova, A., Pramanik, G., Cai, J.-M., Algara-Siller, G., et al., 2013. Nano Lett. 13, 3305–3309.
Bai, L.J., Yuan, R., Chai, Y.Q., et al., 2012. Biomaterials 33, 1090–1096.
Bi, S., Zhang, J., Hao, L., Ding, S.Y., et al., 2011. Anal. Chem. 83, 3696–3702.
Bu, N.N., Tang, C.X., He, X.W., et al., 2011. Chem. Commun. 47, 7689–7691.
Cao, J., Feng, C., Liu, Y., et al., 2014. Biosens. Bioelectron. 57, 133–138.
Dong, J., Cui, X., Deng, Y., et al., 2012. Biosens. Bioelectron. 38, 258–263.
Ghasemi, Farhad, Wegman, David W., Kanoatov, Mirzo, et al., 2013. Anal. Chem. 85, 10062–10066.
Ge, Z., Lin, M., Wang, P., et al., 2014. Anal. Chem. 86, 2124–2130.
Huang, F.J., You, M.X., Han, D., et al., 2013. J. Am. Chem. Soc. 135, 7967–7973.
Kristina, M., Herbert, Genaro Pimienta, et al., 2013. Cell Rep. 5, 1070–1081.
Liu, S.F., Lin, Y., Liu, T., et al., 2014. Biosens. Bioelectron. 56, 12–18.
Ma, C.X., Liang, M., Wang, L., et al., 2013. Biosens. Bioelectron. 47, 467–474.
Mao, X., Ma, Y.Q., Zhang, A.G., et al., 2009. Anal. Chem. 81, 1660–1668.
Singh, Meenakshi, Holzinger, Michael, Biloivan, Olga, et al., 2013. Carbon 61, 349–356.
Pei, H., Lu, N., Wen, Y.L., et al., 2010. Adv. Mater. 22, 4754–4758.
Pei, H., Zuo, X.L., Pan, D., et al., 2013. NPG Asia Mater. 5, e51.
Peltier, H.J., Latham, G.J., 2008. RNA 14, 844–852.
Ryoo, S.R., Lee, J., Yeo, J., et al., 2013. ACS Nano 7, 5882–5891.
Shi, C., Liu, Q., Ma, C.X., et al., 2014. Anal. Chem. 86, 336–339.
Song, C., Xie, G.M., Wang, L., et al., 2014. Biosens. Bioelectron. 58, 68–74.
Tian, K., He, Z.J., Wang, Y., et al., 2013. ACS nano 7, 3962–3969.
Wen, Y.L., Pei, H., Wan, Y., et al., 2011. Anal. Chem. 83, 7418–7423.
Xu, M.D., Zhuang, J.Y., Chen, X., et al., 2013. Chem. Commun. 49, 7304–7306.
Yin, B.C., Liu, Y.Q., Ye, B.C., 2013. Anal. Chem. 85, 11487–11493.
Yuan, Y.L., Chai, Y.Q., Yuan, R., et al., 2013. Chem. Commun. 49, 7328–7330.
Zhang, B., Liu, B.Q., Tang, D.P., et al., 2012. Anal. Chem. 84, 5392–5399.
Zhang, X.Y., Wang, Y., Brandon, L.F., et al., 2014. ACS Nano 8, 3444–3450.
Zhou, J., Lai, W.Q., Zhuang, J.Y., et al., 2013. ACS Appl. Mater. Interfaces 5, 2773–2781.
Zhou, W.J., Chen, Y., Corn, R.M., 2011. Anal. Chem. 83, 3897–3902.